frontiers | Frontiers in Physics

TYPE Original Research
PUBLISHED 04 October 2022
DOI 10.3389/fphy.2022.1007989

OPEN ACCESS

EDITED BY
Peter Fischer,
Berkeley Lab (DOE), United States

REVIEWED BY
Na Lei,
Beihang University, China
Pavel Lukashev,
University of Northern Iowa,
United States

*CORRESPONDENCE
Atsufumi Hirohata,
atsufumi.hirohata@york.ac.uk

SPECIALTY SECTION
This article was submitted to Condensed Matter Physics, a section of the journal Frontiers in Physics

RECEIVED 31 July 2022
ACCEPTED 20 September 2022
PUBLISHED 04 October 2022

CITATION
Hirohata A, Elphick K, Lloyd DC and Mizukami S (2022), Interfacial quality to control tunnelling magnetoresistance. *Front. Phys.* 10:1007989. doi: 10.3389/fphy.2022.1007989

Interfacial quality to control tunnelling magnetoresistance

Atsufumi Hirohata[1]*, Kelvin Elphick[1], David C. Lloyd[1] and Shigemi Mizukami[2,3]

[1]Department of Electronic Engineering, University of York, York, United Kingdom, [2]WPI Advanced Institute for Materials Research, Tohoku University, Sendai, Japan, [3]Center for Science and Innovation in Spintronics (CSIS), Tohoku University, Sendai, Japan

Theoretically, coherent tunnelling through an MgO barrier can achieve over 1,000% magnetoresistance at room temperature. To date, this has not been demonstrated experimentally. In this article, we have categorised magnetic tunnel junctions into four groups and have investigated possible causes of the reduction in their magnetoresistance by correlating their interfacial atomic structures and spin-polarised electron transport. We have concluded that the spin fluctuation induced by dislocations and disordering at a ferromagnet/barrier interface reduced the corresponding magnetoresistance.

KEYWORDS

magnetic tunnel junction (MTJ), tunnelling magnetoresistance (TMR) ratio, interfacial disordering, dislocations, lattice matching

Introduction

Current information technology heavily relies on semiconductor-based nanoelectronics. In order to sustain the improvement of semiconductor devices, post-Moore technologies need to be developed. Spintronics can offer alternative devices utilising the spin polarisation of electrons and holes as an additional degree of freedom. This can offer low-energy device operation and non-volatile data storage.

The major difference between current nanoelectronics and spintronics is the importance of their interfaces [1]. In semiconductor nanoelectronics, a depletion layer, the thickness of which can be up to the order of μm, is intrinsically formed by attaching a metallic contact and a semiconducting layer. This reduces the importance of the interfacial smoothness and quality. Spintronics, on the other hand, requires an atomically sharp interface to minimise spin-dependent and -independent electron scattering caused by ferromagnetic and non-magnetic contaminants in the vicinity of an interface; which reduces the magnitude of a spin-polarised electrical current induced in the system and the resulting efficiency for operation [2, 3]. Accordingly, the importance of the interface control has been increasing significantly in recent years.

In this study, we employed magnetic tunnel junctions (MTJs), which are the most commonly used spintronic devices for memory and recording applications as well as future applications as a magnetic switch. We categorised MTJs into four (A) polycrystalline, (B) epitaxial (C) lattice softened and (D) lattice matched (without dislocations) MTJs as listed in Table 1, and characterised the differences in their interfaces using cross-sectional transmission electron microscopy (TEM). These

TABLE 1 List of properties for four major MTJs.

MTJ types	(A) polycrystalline	(B) Epitaxial		(C) Lattice-softened	(D) Lattice-matched
		(B1) Epitaxial growth	(B2) Amorphous growth		
Barriers	Al-O	MgO	MgO	MgO	MgAl-O
Examples	Co/Al-O/Co	Fe/MgO/Fe $Co_2Mn_{0.74}Ge_{0.43}$/MgO/$Co_{0.5}Fe_{0.5}$	$Co_{0.2}Fe_{0.6}B_{0.2}$/MgO/$Co_{0.2}Fe_{0.6}B_{0.2}$	$Co_{0.75}Mn_{0.25}$/MgO/$Co_{0.75}Mn_{0.25}$	Fe/$MgAl_2O_4$/Fe
Grain boundaries	Dominant	Minor	Minor	Minor	Negligible
Interfacial defects	Dominant	Dominant	Minor	Minor	Negligible
Atomic disorder, void and contaminations	Dominant	Major	Major	Minor	Negligible
Different crystalline orientations	Dominant	Minor	Minor	Minor	Negligible
Lattice strain and deformation	Minor	Major	Minor	Negligible	Negligible
Maximum TMR ratio reported at room temperature (RT) (%)	81 [$Co_{0.4}Fe_{0.4}B_{0.2}$ (3)/Al (0.6)-Ox/$Co_{0.4}Fe_{0.4}B_{0.2}$ (2.5) (thickness in nm)] [4]	429 [Co_2 $Mn_{1.24}Fe_{0.16}Si_{0.84}$ (3)/MgO (2.9)/Co_2 $Mn_{1.24}Fe_{0.16}Si_{0.84}$ (3) (thickness in nm)] [5]	604 [$Co_{0.2}Fe_{0.6}B_{0.2}$ (6)/MgO (2.1)/$Co_{0.2}Fe_{0.6}B_{0.2}$ (4) (thickness in nm)] [6]	229 [$Co_{0.75}Mn_{0.25}$ (10)/MgO (2.4)/$Co_{0.75}Mn_{0.25}$ (4) (thickness in nm)] [7]	429 [Fe (50)/Mg (0.5)/$MgAl_2O_4$ (1.8)-OxFe (5) (thickness in nm)] [8]

interfaces were correlated with their spin transport, revealing the controlling parameters at the interfaces. Our findings can be fed back to the growth and fabrication processes of MTJs for their optimisation and improvement.

Experimental procedures

MTJ samples were prepared using ultrahigh vacuum magnetron sputtering. MgO(001) single crystal and thermally oxidised substrates were used for the deposition of MTJ consisting of Cr (40)/$Co_{0.5}Fe_{0.5}$ (10)/MgO (2)/$Co_{0.5}Fe_{0.5}$ (4)/IrMn (10)/Ru (5), Ta (5)/Ru (10)/Ta (5)/$Co_{0.2}Fe_{0.6}B_{0.2}$ (10)/MgO (2)/$Co_{0.2}Fe_{0.6}B_{0.2}$ (2)/Ta (3)/Ru (5) and Cr (40)/$Co_{0.83}Mn_{0.17}$ (10)/MgO (2.4)/$Co_{0.83}Mn_{0.17}$ (4)/Co_3Fe (1.5)/IrMn (10)/Ru (5) (thickness in nm) with a Ti and Au top electrode. *In-situ* annealing was carried out after the deposition of the Cr seed layer and $Co_{0.83}Mn_{0.17}$ layers at 700°C and 200°C for 1 h, respectively. MTJs were then post-annealed at 325°C for their crystallisation after patterned into pillars with Ti/Au electrodes by photolithography.

The thin film samples were prepared for cross-section TEM imaging *via* mechanical polishing. Mechanical polishing was chosen over focused ion beam techniques because of the fragile nature of the tunnelling barrier material and to preserve interfacial crystallinity that would otherwise be damaged by gallium ion implantation. Diced sections of the thin film samples were epoxied together between pieces of silicon. These cross-section stacks were then thinned using lapping pads (15, 6, 3, 1 μm roughness). Final thinning was performed using Ar ion polishing (Gatan PIPS). TEM imaging was then performed with a JEOL JEM-2011 TEM operating at 200 kV accelerating voltage.

Results and discussion

Figure 1 shows representative TEM images of three distinctive MTJs with MgO barriers sandwiched by (B1) conventional ferromagnets (B2) amorphous ferromagnets and (C) soft-lattice ferromagnets. For the conventional ferromagnet, we imaged MTJs consisting of MgO(001)//Cr (40)/$Co_{0.5}Fe_{0.5}$ (10)/MgO (2)/$Co_{0.5}Fe_{0.5}$ (4)/IrMn (10)/Ru (5) (thickness in nm) as shown in Figure 1A together with the corresponding Fourier filtered image in Figure 1B. The MTJs were epitaxially grown on an MgO(001) substrate, which may induce some strain in the $Co_{0.5}Fe_{0.5}$/MgO/$Co_{0.5}Fe_{0.5}$ junctions. The lattice constant of the MgO barrier is also estimated to be 0.430 nm (102% of the bulk value of 0.421 nm [9]). This may induce interfacial strain to top $Co_{0.5}Fe_{0.5}$ layers. The lattice constant of the bottom $Co_{0.5}Fe_{0.5}$ layer is estimated to be 0.291 nm, which is 102% of the bulk value of 0.2849 nm [10]. The total distance which is analysed in the TEM images over the bottom MgO/$Co_{0.5}Fe_{0.5}$ interface is about 68.2 nm. There are eight dislocations due to their lattice mismatch appeared across 68.2 nm. On average this leads to the dislocation density of 8.5 nm^{-1}. The total distance analysed for the top MgO/$Co_{0.5}Fe_{0.5}$ interface is about 72.7 nm. There are six dislocations appeared for this case, resulting the averaged dislocation density of 12.1 nm^{-1}. These dislocations can be the major cause of the interfacial spin fluctuation as discussed below.

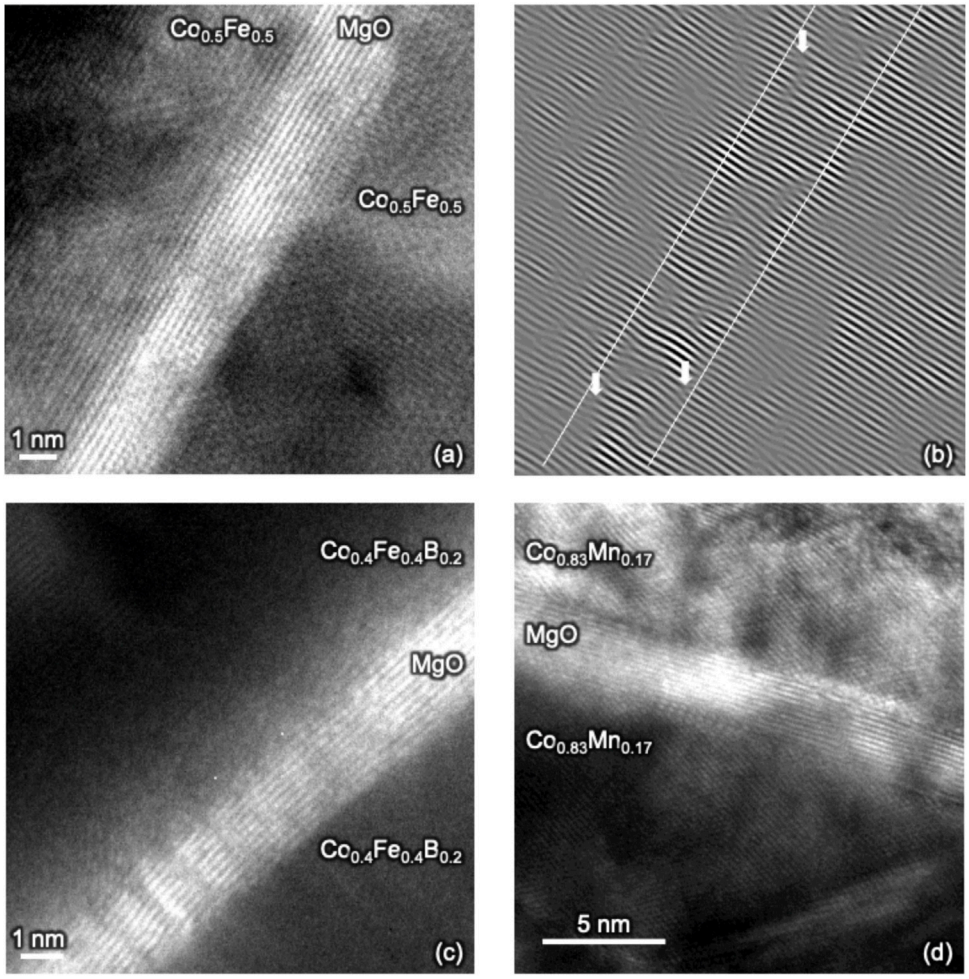

FIGURE 1
Cross-sectional TEM images of three distinctive interfaces; epitaxial MgO barriers with **(A)** conventional $Co_{0.5}Fe_{0.5}$ (**(B)** the corresponding filtered image-white arrows highlight dislocations), **(C)** amorphous $Co_{0.2}Fe_{0.6}B_{0.2}$ and **(D)** strain-free $Co_{0.83}Mn_{0.17}$ ferromagnets.

TABLE 2 List of structural and magnetic properties for MTJs studied.

MTJ types	(B) Epitaxial		(C) Lattice-softened
	(B1) Epitaxial growth	(B2) Amorphous growth	
Samples	$Co_{0.5}Fe_{0.5}$/MgO/$Co_{0.5}Fe_{0.5}$	$Co_{0.2}Fe_{0.6}B_{0.2}$/MgO/$Co_{0.2}Fe_{0.6}B_{0.2}$	Co_xMn_{1-x}/MgO/Co_xMn_{1-x}
Lattice constant of the bottom ferromagnet (nm)	0.291 (102% of bulk value)	0.257 (89.7% of bulk value)	0.283 (x = 0.75) ~ 0.298 (x = 0.86)
Lattice constant of MgO (nm)	0.430 (102% of bulk value)	0.368 (87.5% of bulk value)	0.433 (103% of bulk value)
Lattice constant of the top ferromagnet (nm)	Same as the bottom ferromagnet	Same as the bottom ferromagnet	0.296 (x = 0.75) ~ 0.293 (x = 0.86)
Dislocation density (nm^{-1})	8.5 (bottom) ~ 12.1 (top)	~7.2	11.4 (x = 0.75) ~ 8.9 (x = 0.86)
TMR ratio at RT (%)	75	105	229 (x = 0.75) ~ 120 (x = 0.86)

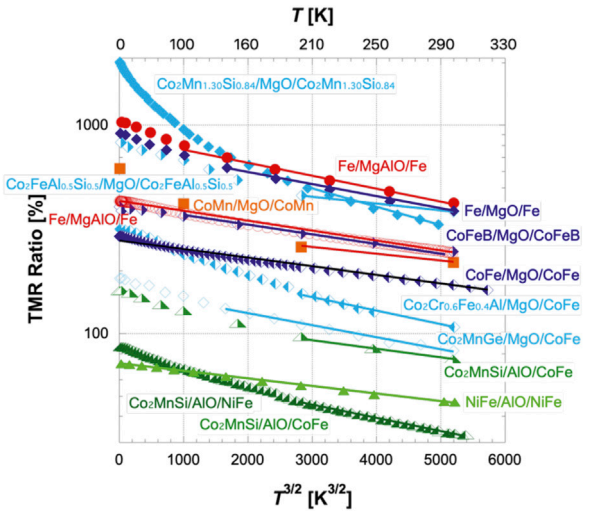

FIGURE 2
Temperature-dependence of TMR ratios of four types of MTJs [12]. Green triangles represent MTJs with Al-O barriers; light closed for $Ni_{0.8}Fe_{0.2}$/Al-O/$Ni_{0.8}Fe_{0.2}$ [13], dark right-filled for Co_2MnSi/Al-O/$Co_{0.5}Fe_{0.5}$ [14], dark left-filled for Co_2MnSi/Al-O/$Ni_{0.8}Fe_{0.2}$ [13] and dark open Co_2MnSi/Al-O/$Co_{0.7}Fe_{0.3}$ [15]. Blue diamonds represent MTJs with MgO barriers; dark closed for Fe/MgO/Fe [8], dark right-filled for $Co_{0.4}Fe_{0.4}B_{0.2}$/MgO/$Co_{0.4}Fe_{0.4}B_{0.2}$ [14], dark left-filled for $Co_{0.84}Fe_{0.16}$/MgO/$Co_{0.84}Fe_{0.16}$ [16], light closed for $Co_2Mn_{1.30}Si_{0.84}$/MgO/$Co_2Mn_{1.30}Si_{0.84}$ [17], light right-filled for $Co_2FeAl_{0.5}Si_{0.5}$/MgO/$Co_2FeAl_{0.5}Si_{0.5}$ [18], light left-filled for $Co_2Fe_{0.6}Cr_{0.4}Al$/Mg-O/$Co_{0.5}Fe_{0.5}$ [19] and light open $Co_2Mn_{0.74}Ge_{0.43}$/MgO/$Co_{0.5}Fe_{0.5}$ [20]. Amber closed squares show strain-free $Co_{0.75}Mn_{0.25}$/MgO/$Co_{0.75}Mn_{0.25}$ [7]. Red closed circles represent MTJs with MgAl-O barriers; closed and open for Fe/$MgAl_2O_4$/Fe [8, 21], respectively.

For the amorphous ferromagnet, we observed MTJs consisting of Si/SiO_2//Ta (5)/Ru (10)/Ta (5)/$Co_{0.2}Fe_{0.6}B_{0.2}$ (10)/MgO (2)/$Co_{0.2}Fe_{0.6}B_{0.2}$ (2)/Ta (3)/Ru (5) (thickness in nm) as seen in Figure 1C. For this type of MTJ, the crystallisation is initiated by the MgO barrier, followed by the crystallisation of the neighbouring $Co_{0.2}Fe_{0.6}B_{0.2}$ layers through their interfaces [11]. The lattice constant of MgO is measured to be 0.368 nm, which is 87.5% of the bulk value. The lattice constant of $Co_{0.2}Fe_{0.6}B_{0.2}$ is estimated to be 0.257 nm, which is the same for the top and bottom interfaces of the MgO barrier. This leads to 89.7% match with the bulk value. The lattice mismatch between $Co_{0.4}Fe_{0.4}B_{0.2}$ and MgO is accordingly calculated to be 1% but with the dislocation density of 7.2 nm^{-1}, which may be due to the formation of grains during the crystallisation. This can minimise any interfacial spin fluctuation on both sides of the MgO barrier unlike MTJs with the conventional ferromagnets as summarised in Table 2.

For strain-free MTJs consisting of MgO(001)//Cr (40)/$Co_{0.83}Mn_{0.17}$ (10)/MgO (2.4)/$Co_{0.83}Mn_{0.17}$ (4)/$Co_{0.75}Fe_{0.25}$ (1.5)/$Ir_{0.25}Mn_{0.75}$ (10)/Ru (5) (thickness in nm)] [7], MTJs were epitaxially grown but the interfacial strain should be absorbed by the lattice deformation. The lattice constant of the MgO barrier is also estimated to be 0.433 nm (103% of the bulk value). Here, the MgO barriers are found to contain some textured grains misaligned to the matrix. Such grains have previously been reported as uncrystallised grains to induce spin-independent hopping but their contribution to spin transport is found to be negligible. This may induce interfacial strain to the top $Co_{0.83}Mn_{0.17}$ layers. The lattice constant of the bottom $Co_{0.83}Mn_{0.17}$ layer is estimated to be 0.294 nm with some periodic dislocations to release the lattice strain induced mainly at the grain boundaries as above, achieving strain-free nature across textured grains. The dislocation density is estimated to be ~10.0 nm^{-1}, which can be further reduced to (11.4 ± 0.3) nm^{-1} for $Co_{0.75}Mn_{0.25}$ for larger tunnelling magnetoresistance (TMR) ratio of 229% at room temperature (RT) and increased to (8.9 ± 0.3) nm^{-1} for $Co_{0.86}Mn_{0.14}$ with smaller TMR ratio of 142% at RT. This again confirms the dislocation density controls the interfacial spin fluctuation and the resulting TMR ratios. By comparing with the $Co_{0.4}Fe_{0.4}B_{0.2}$/MgO interface, the dislocation density and discrepancy between the top and bottom interfaces need to be reduced further to eliminate any spin fluctuation induced by the interfacial dislocations and vacancies in the ferromagnets.

Figure 2 shows the temperature-dependence of TMR ratios [12] with additional data. The data in Figure 2 are categorised into four; MTJs with (A) polycrystalline Al-O barriers, epitaxial MgO barriers with (B1) conventional and (C) strain-free ferromagnets, and (D) lattice-matched MgAl-O barriers whose lattice constants match with those of ferromagnets. For the polycrystalline Al-O-based junctions, the TMR ratios almost follow the empirical Bloch law of the temperature-dependence of magnetisation as $AT^{3/2}$, where A is a constant and T is temperature. For example, the TMR ratios of $Ni_{0.8}Fe_{0.2}$/Al-O/$Ni_{0.8}Fe_{0.2}$ can be fit as (71.11 ± 0.37)–(0.00493 ± 0.00013)$T^{3/2}$ between 4 and 300K [13]. This means that the spin-polarised electron transport in Al-O-based MTJs is governed by the temperature-dependence of the magnetisations of the ferromagnetic layers with the gradient of ~0.005. By replacing one of the $Ni_{0.8}Fe_{0.2}$ layers with a Co_2MnSi Heusler-alloy film, the temperature dependence shows faster decrease with increasing T below 200K, leading to the TMR ratio fit as (62.46 ± 0.46)–(0.00571 ± 0.00011)$T^{3/2}$ (200–300K) [13], which increases the gradient of the temperature dependence (>0.005). Here, the Curie temperature of Co_2MnSi (985K for bulk [22]) is higher than that of $Ni_{0.8}Fe_{0.2}$ (850–872K for bulk [23]), and hence this change in gradient can be attributed to an additional factor which controls the spin transport especially at low temperature as discussed later. A similar MTJ consisting of Co_2MnSi/Al-O/CoFe shows a similar trend as (62.22 ± 0.40)–(0.00571 ± 0.00001)$T^{3/2}$ (200–300K) [15].

By replacing polycrystalline Al-O with epitaxial MgO, coherent tunnelling was achieved [16, 24] as theoretically predicted [25, 26]. Although the resulting TMR ratios increase

one order of magnitude, their temperature dependence show similar decrease as that observed for the Al-O-based MTJs with Heusler-alloy films as a ferromagnet below ~100K. For example, a most commonly used MTJs consisting of $Co_{0.4}Fe_{0.4}B_{0.2}$/MgO/$Co_{0.4}Fe_{0.4}B_{0.2}$ can be fit as TMR ratio = (387.20 ± 6.84)–(0.0281 ± 0.0021)$T^{3/2}$ (100–300K) [16], showing larger gradient of 0.02–0.03 than that for Al-O-based MTJ by almost one order of magnitude. Here, the Curie temperature of $Co_{0.4}Fe_{0.4}B_{0.2}$ has been reported to be 750–895K in a film form [27], which is similar to that of $Ni_{0.8}Fe_{0.2}$, excluding the contributions of the magnetisation changes within this temperature range. Similarly, $Co_{0.84}Fe_{0.16}$/MgO/$Co_{0.84}Fe_{0.16}$ follows (266.52 ± 1.22)–(0.0192 ± 0.0004)$T^{3/2}$ (80–300K) [16]. By replacing one of the $Co_{0.84}Fe_{0.16}$ layers with Co_2MnGe Heusler alloy, $Co_2Mn_{0.74}Ge_{0.43}$/MgO/$Co_{0.5}Fe_{0.5}$ again reveals the increase in the gradient as (151.62 ± 2.62)–(0.0139 ± 0.0007)$T^{3/2}$ (140–300K) [20], maintaining the gradient at the same order (Curie temperature of bulk Co_2MnGe: 905K [22]). By using both ferromagnets as Co_2MnSi Heusler alloys, $Co_2Mn_{1.30}Si_{0.84}$/MgO/$Co_2Mn_{1.30}Si_{0.84}$ can be fit as (725.84 ± 17.35)–(0.08063 ± 0.00432)$T^{3/2}$ (200–300K) [17], doubling the gradient as compared with the conventional MgO-based MTJs as above. This suggests additional atomic disorder in the Heusler alloys in the vicinity of the MgO interfaces may induce further spin fluctuation.

In such MgO-based MTJs, the crystallisation is typically initiated in MgO for $Co_{0.4}Fe_{0.4}B_{0.2}$/MgO/$Co_{0.4}Fe_{0.4}B_{0.2}$ and epitaxial growth *via* seed layers is used for the other MTJs. These crystallisation processes may induce strain in the ferromagnetic layers and the tunnel barrier, which may modify their magnetic properties and induce some defects at their interfaces. In order to avoid these issues, lattice-softening of CoMn and MgO layers has been investigated recently [7]. For $Co_{0.75}Mn_{0.25}$/MgO/$Co_{0.75}Mn_{0.25}$, the TMR ratios are fit as 308.98–0.01732$T^{3/2}$. This reduces the gradient of the $T^{3/2}$ dependence slightly as compared with the abovementioned conventional MgO-based MTJs, indicating the contributions of the change in the ferromagnet magnetisations and the interfacial spin fluctuation may contribute dominantly to the reduction of the TMR ratios.

Further improvement of the ferromagnet/barrier interfaces has been demonstrated by doping the MgO barriers with Al to match their lattice constants with the neighbouring ferromagnets perfectly [21]. They fabricated a set of MTJs consisting of Fe/MgO/Fe with and without the Al doping. Fe/MgO/Fe follows (762.96 ± 23.95)–(0.07714 ± 0.00726)$T^{3/2}$ (100–300K), while Fe/MgAl-O/Fe shows (770.53 ± 16.59)–(0.06777 ± 0.000424)$T^{3/2}$ (140–300K). This confirms the elimination of the interfacial defects and associated spin fluctuation can improve the spin transport through MTJs.

For further clarification, the temperature-dependence of conductance for the (anti-)parallel configurations [$G_{P\ (AP)}$]

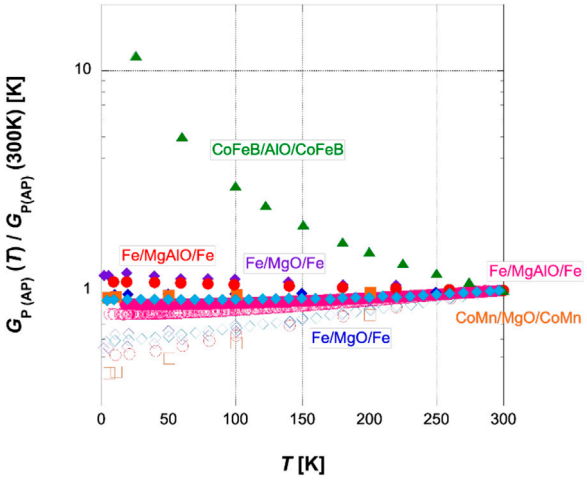

FIGURE 3
Normalised temperature-dependence of conductance for (anti-)parallel magnetisation configurations [$G_{P\ (AP)}$, for closed (open) symbols] of four types of MTJs. Green triangles show $Co_{0.4}Fe_{0.4}B_{0.2}$/Al-O/$Co_{0.4}Fe_{0.4}B_{0.2}$ [29]. Blue and purple diamonds represent MTJs with MgO barriers; Fe/MgO/Fe [8, 30], and light blue diamonds for $Co_2Mn_{0.74}Ge_{0.43}$/MgO/$Co_{0.5}Fe_{0.5}$ [31]. Amber squares show strain-free $Co_{0.75}Mn_{0.25}$/MgO/$Co_{0.75}Mn_{0.25}$ [7]. Red circles show Fe/$MgAl_2O_4$/Fe [8].

from some of the data in Figure 2 are used for fitting with Shang's model [28]:

$$G_{P(AP)} = G_0 \frac{CT}{\sin CT}\left[1 \underset{(-)}{+} P_0^2\{1 - AT^{3/2}\}^2\right] + BT^{4/3}$$

As shown in Figure 3, G_P shows much stronger temperature dependence than G_{AP}. For Co/Al-O/Co and $Ni_{0.8}Fe_{0.2}$/Al-O/$Ni_{0.8}Fe_{0.2}$, A = (1–6) × 10^{-6} $K^{-3/2}$ and (3–5) × 10^{-5} $K^{-3/2}$, which is almost a half of the bulk value A = 1.23 × 10^{-5} $K^{-3/2}$ ($Ni_{0.8}Fe_{0.2}$) [28]. P_0 is estimated to be (34 ± 2)% for Co and (42 ± 3)% for $Ni_{0.8}Fe_{0.2}$.

For Fe/MgO/Fe, A is estimated to be 7.0 × 10^{-6} $K^{-3/2}$, which is ~20% smaller than the bulk Fe value of 9.2 × 10^{-6} $K^{-3/2}$ [30]. This improvement as compared with the polycrystalline Al-O-based MTJs again confirms minor effects of the interfacial quality on spin transport. By using the strain-free $Co_{0.75}Mn_{0.25}$/MgO/$Co_{0.75}Mn_{0.25}$, A is obtained as 1.7 × 10^{-5} $K^{-3/2}$ with P_0 = 0.87, B = (1.688 ± 0.007) × 10^{-10} S·$K^{4/3}$, C = 1.4 × 10^{-3} and G_0 = 1.62 × 10^{-6} S/μm^2 (20 μm^2 squared MTJs) [7].

Further improvement in the interfacial quality can be achieved by using a lattice-matched barrier as $Co_{0.4}Fe_{0.4}B_{0.2}$/$MgAl_2O_4$/$Co_{0.4}Fe_{0.4}B_{0.2}$. For $MgAl_2O_4$-based MTJs (Mg thickness: t_{Mg} = 0.5 nm), B and C are estimated to be 2.031 × 10^8 S·$K^{-4/3}$ and 1.67 × 10^{-3} K^{-1}, leading to the ratio between spin dependent and independent parts: B/G_0 = 1.14 × 10^{-4} [32]. These fitting parameters are listed in Table 3.

TABLE 3 List of fitting parameters for four major MTJs.

MTJ types	(A) polycrystalline	(B) Epitaxial		(C) Lattice-softened	(D) Lattice-matched
		Epitaxial growth	Amorphous growth		
Typical interfacial dislocation density (nm^{-1})	—	8.5–12.1	—	8.9–11.4	—
$T^{3/2}$ fit (K)	4–300	100–300	100–300	200–300	100–300
G_0 (S)	—	—	—	~3×10^6	—
A ($K^{3/2}$)	$10^{-5} \sim 10^{-6}$	$(7–9) \times 10^{-6}$	—	—	—
B($S \cdot K^{4/3}$)	—	—	—	~2×10^{-10}	~2×108
C	—	—	—	~1×10^{-3}	~2×10^{-3}

Table 3 confirms that the initially amorphous MTJs can minimise dislocations and disordering at a MgO interface. However, the spin polarisation of $Co_{0.4}Fe_{0.4}B_{0.2}$ limits the maximum TMR ratio to be 604% at RT. Their temperature dependence follows the empirical $T^{3/2}$ law within a broad temperature range. In order to increase the TMR ratios at RT further to achieve a magnetic switch (TMR ratio >1,000%), highly spin-polarised ferromagnets, such as a Heusler alloy, needs to be used in MTJs, which indeed show >1,000% TMR ratios at low temperature. However, such half-metallicity in a ferromagnet can be broken by atomic disordering induced by defects and dislocations in the vicinity of a neighbouring layer, which consists of different elements, inducing spin fluctuation to reduce TMR ratios at finite temperature. Such interfacial spin fluctuation can be minimised by developing a half-metallic ferromagnet which can be crystallised by MgO as similar to $Co_{0.4}Fe_{0.4}B_{0.2}$ or by improving the interfacial matching with the $MgAl_2O_4$ tunnelling barrier.

Summary

Four groups of magnetic tunnel junctions have been analysed using cross-section TEM, this revealed that the reduction of interfacial dislocations and disorder, increases the corresponding tunnelling magnetoresistance. To date, the minimum dislocation density has been achieved at a $Co_{0.2}Fe_{0.6}B_{0.2}$/MgO interface, which accordingly shows the largest magnetoresistance at room temperature. This has been demonstrated by the post-annealing of an amorphous junction rather than growing a junction epitaxially. On the other hand, a half-metallic ferromagnet has shown larger magnetoresistance at low temperature but the disordered phases formed at MgO interfaces induces spin fluctuation with increasing temperature. For the improvement of the magnetoresistance, it is critical to eliminate such interfacial dislocations and disordering.

Data availability statement

The original contributions presented in the study are included in the article/supplementary material, further inquiries can be directed to the corresponding author.

Author contributions

SM prepared all the samples and performed all the magnetic measurements. KE and DL carried out all the structural analysis. AH initiated this work and made all the data analysis as well as comparison with the earlier works together with the other authors.

Funding

The authors thank our fruitful discussion with Jun-ichiro Inoue. This work is partially supported by EPSRC (EP/V007211/1), JST CREST (JPMJCR17J5) and Royal Society International Exchange grants. SM. thanks CSRN in CSIS at Tohoku University.

Conflict of interest

The authors declare that the research was conducted in the absence of any commercial or financial relationships that could be construed as a potential conflict of interest.

Publisher's note

References

1. Hirohata A, Elphick K, Kubota T, Takanashi K. Applications to nano- and micro-systems. In: A Yamaguchi, A Hirohata, B Stadler, editors. *Nanomagnetic materials: Fabrication, characterization and application*. Amsterdam, Netherlands: Elsevier (2021). p. 11–5.

2. Hirohata A, Yamada K, Nakatani Y, Prejbeanu L, Diény B, Pirro P, et al. Review on spintronics: Principles and device applications. *J Magn Magn Mater* (2020) 509: 166711. doi:10.1016/j.jmmm.2020.166711

3. Dieny B, Prejbeanu IL, Garello K, Gambardella P, Freitas P, Lehndorff R, et al. Opportunities and challenges for spintronics in the microelectronics industry. *Nat Electron* (2020) 3:446–59. doi:10.1038/s41928-020-0461-5

4. Wei HX, Qin QH, Ma M, Sharif R, Han XF. 80% tunneling magnetoresistance at room temperature for thin Al-O barrier magnetic tunnel junction with CoFeB as free and reference layers. *J Appl Phys* (2007) 101:09B501. doi:10.1063/1.2696590

5. Liu H, Kawami T, Moges K, Uemura T, Yamamoto M, Shi F, et al. Influence of film composition in quaternary Heusler alloy Co_2(Mn, Fe)Si thin films on tunnelling magnetoresistance of Co_2(Mn, Fe)Si/MgO-based magnetic tunnel junctions. *J Phys D Appl Phys* (2015) 48:164001. doi:10.1088/0022-3727/48/16/164001

6. Ikeda S, Hayakawa J, Ashizawa Y, Lee YM, Miura K, Hasegawa H, et al. Tunnel magnetoresistance of 604% at 300 K by suppression of Ta diffusion in CoFeB/MgO/CoFeB pseudo-spin-valves annealed at high temperature. *Appl Phys Lett* (2008) 93: 082508. doi:10.1063/1.2976435

7. Elphick K, Yoshida K, Roy T, Ichinose T, Kunimatsu K, Tsuchiya T, et al. Lattice softening in metastable bcc Co_xMn_{100-x} (001) ferromagnetic layers for a strain-free magnetic tunnel junction. *Phys Rev Appl* (2021) 16:054052. doi:10.1103/PhysRevApplied.16.054052

8. Scheike T, Wen Z, Sukegawa H, Mitani S. Enhanced tunnel magnetoresistance in Fe/Mg_4Al-O_x/Fe(001) magnetic tunnel junctions. *Appl Phys Lett* (2022) 120: 032404. doi:10.1063/5.0082715

9. Al-Abadleh HA, Grassian VH. Oxide surfaces as environmental interfaces. *Surf Sci Rep* (2003) 52:63–161. doi:10.1016/j.surfrep.2003.09.001

10. Lee AJ, Ahmed AS, Guo S, Esser BD, McComb DW, Yang F. Epitaxial $Co_{50}Fe_{50}$(110)/Pt(111) films on $MgAl_2O_4$(001) and its enhancement of perpendicular magnetic anisotropy. *J Appl Phys* (2019) 125:183903. doi:10.1063/1.5093503

11. Takeuchi T, Tsunekawa K, Choi Y-S, Nagamine Y, Djayaprawira DD, Genseki A, et al. Crystallization of amorphous CoFeB ferromagnetic layers in CoFeB/MgO/CoFeB magnetic tunnel junctions. *Jpn J Appl Phys* (2007) 46:L623–6. doi:10.1143/JJAP.46.L623

12. Elphick K, Frost W, Samiepour M, Kubota T, Takanashi K, Sukegawa H, et al. Heusler alloys for spintronic devices: Review on recent development and future perspectives. *Sci Technol Adv Mater* (2020) 22:235–71. doi:10.1080/14686996.2020.1812364

13. Schmalhorst J, Kämmerer S, Sacher M, Reiss G, Hütten A, Scholl A. Interface structure and magnetism of magnetic tunnel junctions with a Co_2MnSi electrode. *Phys Rev B* (2004) 70:024426. doi:10.1103/PhysRevB.70.024426

14. Tsunegi S, Sakuraba Y, Oogane M, Takanashi K, Ando Y. Large tunnel magnetoresistance in magnetic tunnel junctions using a Co_2MnSi Heusler alloy electrode and a MgO barrier. *Appl Phys Lett* (2008) 93:112506. doi:10.1063/1.2987516

15. Kämmerer S, Thomas A, Hütten A, Reiss G. Co_2MnSi Heusler alloy as magnetic electrodes in magnetic tunnel junctions. *Appl Phys Lett* (2004) 85:79–81. doi:10.1063/1.1769082

16. Parkin SSP, Kaiser C, Panchula A, Rice PM, Hughes B, Samant M, et al. Giant tunnelling magnetoresistance at room temperature with MgO (100) tunnel barriers. *Nat Mater* (2004) 3:862–7. doi:10.1038/nmat1256

17. Liu H-X, Honda Y, Taira T, Matsuda K, Arita M, Uemura T, et al. Co_2MnSi/MgO/Co_2MnSi magnetic tunnel junctions by half-metallicity of Co_2MnSi and coherent tunnelling. *Appl Phys Lett* (2012) 101:132418. doi:10.1063/1.4755773

18. Tezuka N, Ikeda N, Mitsuhashi F, Sugimoto S. Improved tunnel magnetoresistance of magnetic tunnel junctions with Heusler $Co_2FeAl_{0.5}Si_{0.5}$ electrodes fabricated by molecular beam epitaxy. *Appl Phys Lett* (2009) 94: 162504. doi:10.1063/1.3116717

19. Marukame T, Ishikawa T, Hakamata S, Matsuda K, Uemura T, Yamamoto M. Highly spin-polarized tunneling in fully epitaxial $Co_2Cr_{0.6}Fe_{0.4}$Al/MgO/$Co_{50}Fe_{50}$ magnetic tunnel junctions with exchange biasing. *Appl Phys Lett* (2007) 90:012508. doi:10.1063/1.2428412

20. Hakamata S, Ishikawa T, Marukame T, Matsuda K, Uemura T, Arita M, et al. Improved tunnel magnetoresistance characteristics of magnetic tunnel junctions with a Heusler alloy thin film of Co_2MnGe and a MgO tunnel barrier. *J Appl Phys* (2007) 101:09J513. doi:10.1063/1.2713209

21. Belmoubarik M, Sukegawa H, Ohkubo T, Mitani S, Hono K. $MgAl_2O_4$(001) based magnetic tunnel junctions made by direct sputtering of a sintered spinel target. *Appl Phys Lett* (2016) 108:132404. doi:10.1063/1.4945049

22. Webster PJ, Ziebeck KRA. Heusler alloys. In: HPJ Wijn, editor. *Landolt-börnstein new series group III*, 19. Berlin, Germany: Springer (1988). p. 75. doi:10.1007/10353201_49

23. Wakelin RJ, Yates EL. A study of the order-disorder transformation in iron-nickel alloys in the region $FeNi_3$. *Proc Phys Soc B* (1953) 66:221–40. doi:10.1088/0370-1301/66/3/310

24. Yuasa S, Nagahama T, Fukushima A, Suzuki Y, Ando K. Giant room-temperature magnetoresistance in single-crystal Fe/MgO/Fe magnetic tunnel junctions. *Nat Mater* (2004) 3:868–71. doi:10.1038/nmat1257

25. Butler WH, Zhang X-G, Schulthess TC, MacLaren JM. Spin-dependent tunneling conductance of Fe|MgO|Fe sandwiches. *Phys Rev B* (2001) 63:054416. doi:10.1103/PhysRevB.63.054416

26. Mathon J, Umerski A. Theory of tunneling magnetoresistance of an epitaxial Fe/MgO/Fe(001) junction. *Phys Rev B* (2001) 63:220403. doi:10.1103/PhysRevB.63.220403

27. Lee K-M, Choi JW, Sok J, Min B-C. Temperature dependence of the interfacial magnetic anisotropy in W/CoFeB/MgO. *AIP Adv* (2017) 7:065107. doi:10.1063/1.4985720

28. Shang CH, Nowak J, Jansen R, Moodera JS. Temperature dependence of magnetoresistance and surface magnetization in ferromagnetic tunnel junctions. *Phys Rev B* (1998) 58:R2917–20. doi:10.1103/PhysRevB.58.R2917

29. Mazumdar D, Liu X, Schrag BD, Shen W, Carter M, Xiao G. Thermal stability, sensitivity, and noise characteristics of MgO-based magnetic tunnel junctions (invited). *J Appl Phys* (2007) 101:09B502. doi:10.1063/1.2710953

30. Wang SG, Ward RCC, Du GX, Han XF, Wang C, Kohn A. Temperature dependence of giant tunnel magnetoresistance in epitaxial Fe/MgO/Fe magnetic tunnel junctions. *Phys Rev B* (2008) 78:180411. doi:10.1103/PhysRevB.78.180411

31. Ishikawa T, Marukame T, Kijima H, Matsuda K-I, Uemura T, Arita M, et al. Spin-dependent tunneling characteristics of fully epitaxial magnetic tunneling junctions with a full-Heusler alloy Co_2MnSi thin film and a MgO tunnel barrier. *Appl Phys Lett* (2006) 89:192505. doi:10.1063/1.2378397

32. Liu H, Ma Q, Rizwan S, Liu D, Wang S, Han X. Tunnel magnetoresistance effect in CoFeB/MgAlO/CoFeB magnetic tunnel junctions. *IEEE Trans Magn* (2011) 47:2716–9. doi:10.1109/TMAG.2011.2157814